Carbonates and Evaporites (2022) 37:78
https://doi.org/10.1007/s13146-022-00823-z

ORIGINAL ARTICLE

Petrofacies and diagenesis of Thanetian Lockhart Limestone in the Upper Indus Basin (Pakistan): implications for the Ceno-Tethys Ocean

Ahmer Bilal[1,3] · Renchao Yang[1,2] · Aiping Fan[1] · Muhammad Saleem Mughal[3] · Yang Li[1] · Muhammad Basharat[3] · Muhammad Farooq[3]

Accepted: 26 October 2022 / Published online: 2 November 2022

Abstract

An integrated study based on petrography, SEM and XRD analysis has been carried out for petrofacies and diagenesis of the Lockhart Limestone in the Upper Indus Basin, Pakistan to decipher the paleo-environmental history during the mature development of the Ceno-Tethys Ocean. The Thanetian Lockhart Limestone has been divided into three petrofacies referred as: mudstone (CMF-I), mudstone to wackestone (CMF-II), and wackestone to packstone (CMF-III). These petrofacies deposited in the transgressive environment of the Ceno-Tethys Ocean along the toe of the carbonate platform's slope, slope, and shelf areas, respectively. In the Thanetian Limestone, three diagenetic stages indicated by their respective types of cementing material i.e., CMF-I demonstrates eogenesis with the appearance of drusy cement, CMF-II shows both mesogenesis and telogenesis, revealed by the blocky and rim cement, while CMF-III displays mesogenesis with the presence of blocky cement. These various grades of diagenesis are ultimate directly proportional to the ascending hierarchy of cement generations. Syngenetic-originated cubic pyrite and diagenetically formed framboidal pyrite are confined to the first microfacies (CMF-I), depicting that its deposition took place under a relatively deeper anoxic environment as compared to other microfacies. Compaction, cementation and micritization are the diagenetic impacts responsible for the destruction of primary porosity. While, in contrast, secondary porosity has been generated by epidiagenetic impacts like stylolites, fracturing, dolomitization and dissolution. Hence, these factors have enhanced the reservoir characteristics for Lockhart Limestone as a potential hydrocarbon reservoir rock.

Keywords Cement generations · Ceno-Tethys Ocean · Diagenesis · Microfacies · Palaeoenvironment · Petrography

Introduction

The composition and texture of carbonates can reveal the depositional environment (Wilson 1975; Flugel 2010). The secondary porosity of micritic carbonates is much more reliable due to dissolution features created by shallow shelf percolating CO2-rich meteoric water, which can easily dissolve sparry calcite and other framework grains (Tian et al. 2017). Puguang gas field in the Sichuan Basin, Southern China and the Yates field of western Texas, USA are the best examples of a wealthy fertile reservoir, in which porosity is enhanced due to the development of secondary structures during diagenetic alterations (Xiao et al. 2014). Carbonate rocks undergo percolating episodes of ore-bearing solutions in the fissures and caverns, consequences in the deposition of bituminous carbonate-type uranium deposits, which are hosted in Paleogene carbonates Kyrgyzstan (Prothero and Schwab 2014).

✉ Renchao Yang
yang100808@126.com

Ahmer Bilal
ahmerbilal47@gmail.com

[1] Shandong Provincial Key Laboratory of Depositional Mineralization and Sedimentary Minerals, Shandong University of Science and Technology, Qingdao 266590, China

[2] Laboratory for Marine Mineral Resources, Qingdao National Laboratory for Marine Science and Technology, Qingdao 266071, China

[3] Institute of Geology, University of Azad Jammu and Kashmir, Muzaffarabad 13100, Pakistan

Hydrocarbon discovery from Lockhart Limestone along the Indus Basin of Pakistan develops recent interests in searching of the formation exposure in different parts of the country for the possible conventional or unconventional reservoir presence (Afzal et al. 2009) and to understand the facies variations along freshly mapped areas (Fig. 1). Tectonically sandwich strata near hinterland regions need to be studied in digenetic perspective and in comparison of deeper rocks, which are possibly facing high grade of cooking resultantly creating similar conditions like some major gas producers in the world (Yu et al. 2018). Dissolution in subsurface limestone enhances porosity making it a perfect storage rock for hydrocarbon in half of the world's reservoirs (Baques et al. 2020).

Previous workers carried out reconnaissance studies (Ahmed et al. 2018; Ahsan and Shah 2017; Awais et al. 2019; Khan et al. 2018a, 2020; Naeem et al. 2014; Nawaz et al. 2015), on the Lockhart Limestone of other areas in the Upper Indus Basin. The unconformable lower contact of Lockhart Limestone was marked in the Hazara Kashmir Syntaxis along with a few intra-formational faults (Fig. 1; Bilal et al. 2022; Shah et al. 2020). It is a positive signature that unconformity has played an important role as a stratigraphic trap in some parts of the world (Zhu et al. 2020), as well as faults also act as sealing for the hydrocarbon in the surrounding basins of Pakistan and China (Qureshi et al. 2021). In this manuscript, we will try to understand the evolution of diagenesis in Lockhart Limestone with the help of the petrographic and microfacies approach.

Worldwide carbonate rocks were dominated by fine-grained micritic composition but not highly focused on by researchers as compared to easy observable clastic rocks (Cabral et al. 2019), resulting in a partial and incomplete understanding of the micritic limestones, especially when deposits lie right next to the clastic source, which in turn shoot up its complexity (Xia et al. 2019). In the study area, the hyper tectonic Sub-Himalayan conditions influence the Ceno-Tethys deposits of Lockhart Limestone, which were subjected to diagenetic changes and are not studied in detail previously (Fig. 1). Hence, the scheme objective of this paper is to perceive the limestone behavior in response to diagenetic transformations in the strata throughout its genesis along the Ceno-Tethys Ocean followed by high tectonic pressure in later stage, as well as to find out the modern scales to evaluate such evolutionary alterations.

Geological background

Tectonic framework and location of the study area

North East trending Indus Basin (IB) lies in the Himalayan foreland zone and is the largest sedimentary basin of Pakistan (Fig. 1). It extends up to Kurram Thrust from the west, Kohistan Island Arc (KIA) from the north, stable Indian craton to the southeast and runs up to the Indus offshore towards the south (Ehsan et al. 2018). In the eastern part of Pakistan, the basin holds forth to the state of Azad Jammu and Kashmir (AJ&K) and is discredited from high-graded metamorphics by Panjal Thrust (PT) (Bilal et al. 2022). Lesser Himalayas is a prominent division demarcated by the Main Boundary Thrust (MBT) from the south and the Main Central Thrust (MCT) via the North (Bilal et al. 2022; Khan and Clyde 2013). The study area belongs to the base of the Lesser Himalayas (Fig. 1). On the grounds of the existing structural framework and paleo-genetic evolution history, this basin is divided into the Upper Indus Basin (UIB) also known as Kohat Potwar Basin (KPB), and the Lower Indus Basin (Khan and Clyde 2013). UIB is bounded by PT from east and north, Salt Range Thrust via west while Indus River and Kalabagh fault together mark its southern limit (Awais et al. 2019).

The study area falls in the center of Hazara Kashmir Syntaxis (HKS), which is a prominent syntaxial bend in the northeastern part of UIB responsible for the tremendously folded faulted and sandwich strata in the region (Bilal et al. 2022; Qasim et al. 2020). Paleocene strata wrapped along with the limbs of this syntaxis like a half-thin seam of a ball (Fig. 1). Closure events of the Ceno-Tethys Ocean (Metcalfe 2021) have modified the evolution of the study area along with intense events of Laurasia and Gondwana land collision. It is then followed by the uplifting of Tertiary aged Himalayan Orogeny, which finally, in turn, inverts the whole topography in the Cenozoic era (Shah 2009).

Stratigraphy

The stratigraphic sequence (Fig. 2) along the Lesser Himalayan meta-sedimentary region comprised of Precambrian to recent rocks of both marine and non-marine origin (Ahsan and Shah 2017). Ordovician to Carboniferous, alongside Permian to Paleocene as well as Oligocene time, displays prominent unconformities in the region.

Deposition in the Paleocene age, featured in the calcareous dominating hard and thick-bedded nodular Lockhart Limestone with shale intercalations, depicting the lacustrine settling environment of the region at that time (Naeem et al. 2014). Shallow marine inner to outer neritic shelf hosts these fossiliferous carbonates. In the Attock area of the Potwar sub-basin, the reservoir bearing Lockhart Limestone in the Meyal Oil field is reported dominantly as argillaceous (Awais et al. 2019). High visual porosity is observed in the hydrocarbon-producing formation along the Hazara belt (Hasany and Saleem 2012), however, excellent quality hydrocarbon saturation is marked in the Chanda deep-01 well of the Kohat area, with relatively less porosity of 9.5%

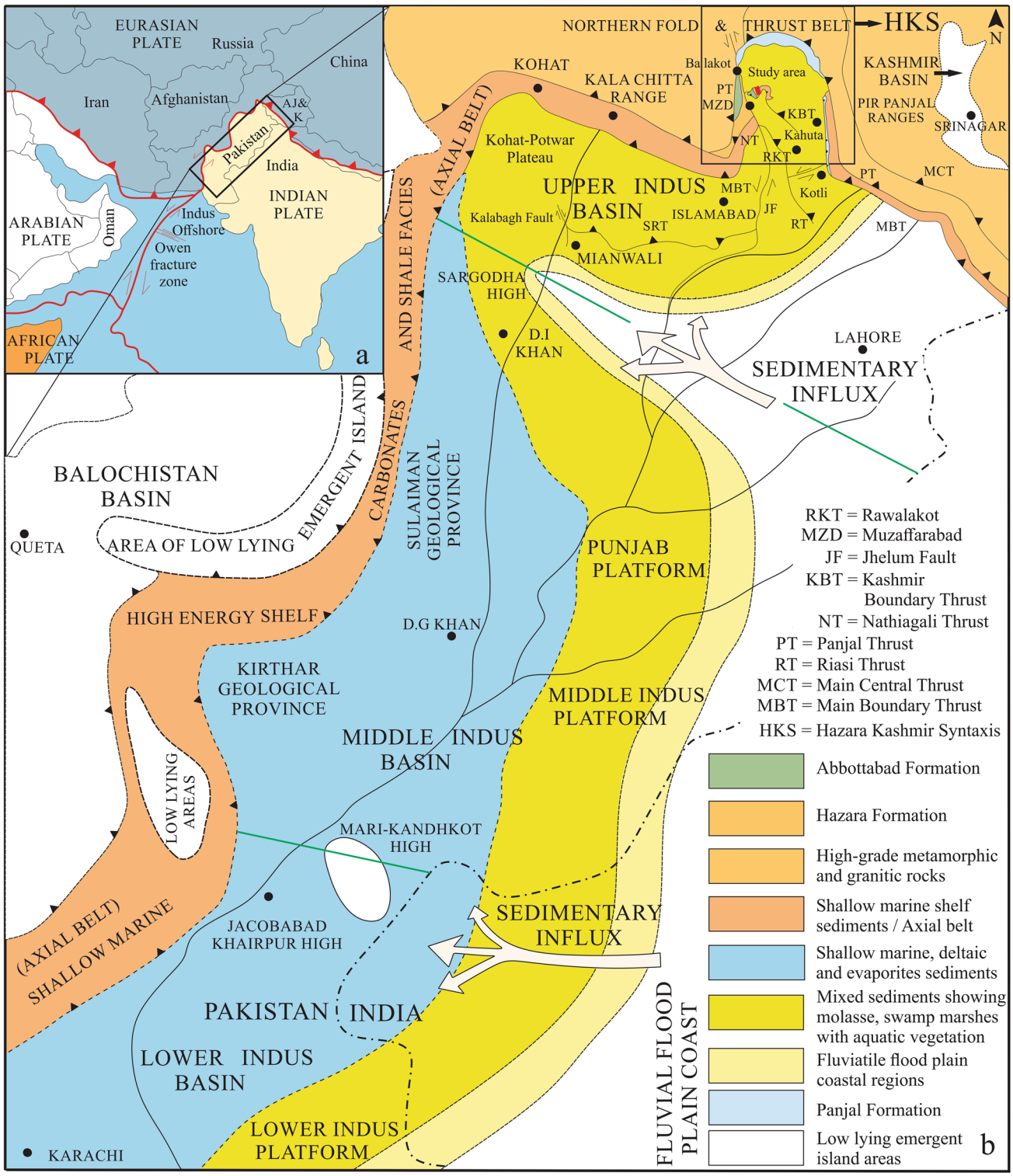

Fig. 1 **a** Large-scale tectonostratigraphic map of Pakistan illustrating regional scale plate boundaries and Indus Basin. **b** Geological map depicting the locations of the Indus Basin and Hazara Kashmir Syntaxis (modified from Shah 2009)

(Nawaz et al. 2015). Moreover, from the Hazara to Kashmir areas porosity of the Lockhart Limestone is reduced considerably from 25 to 11% (Ahsan and Shah 2017), respectively. This is because the Hazara is present on the limbs and the Kashmir area is present in the core of the Hazara- Kashmir Syntaxis.

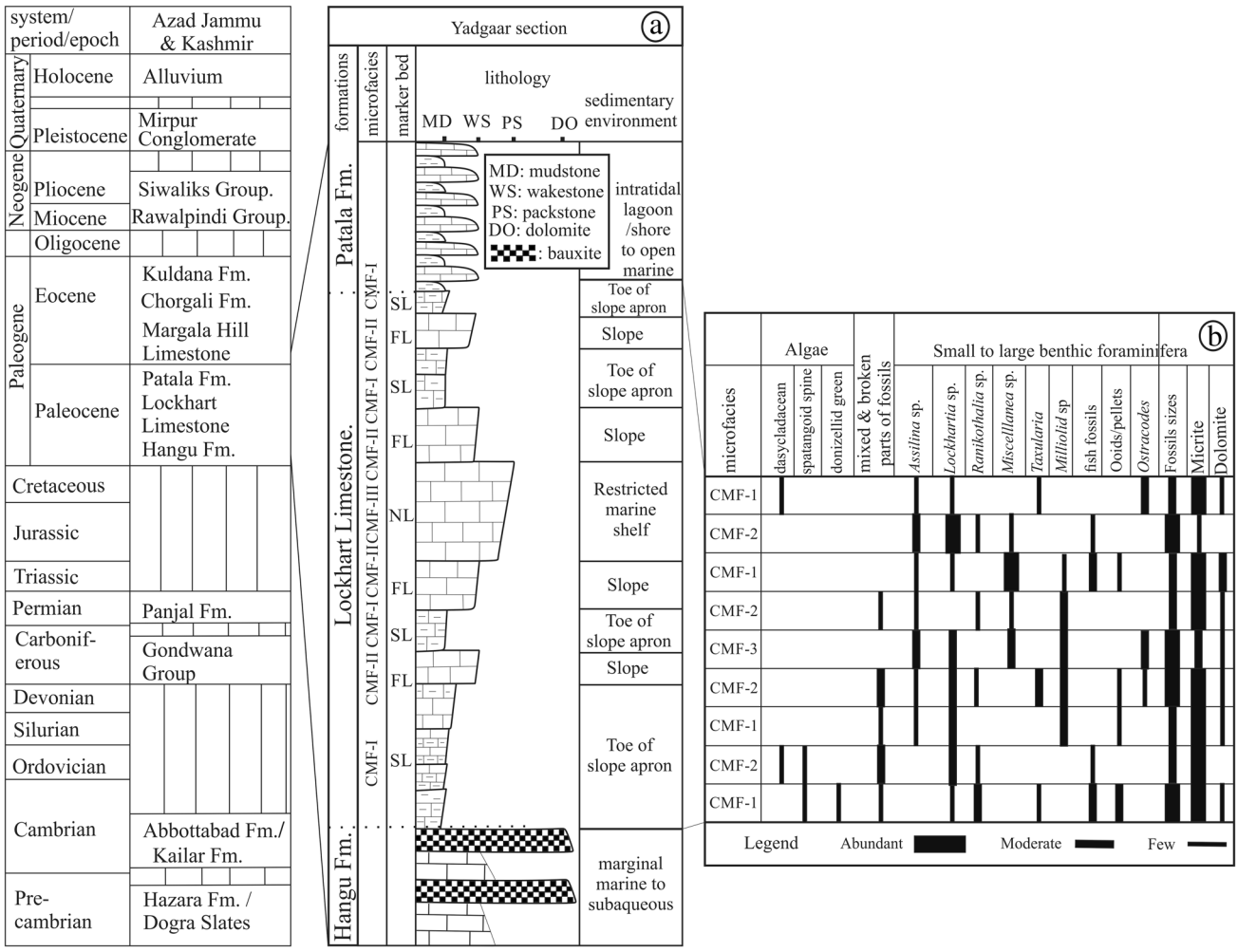

Fig. 2 Stratigraphic succession of the study area in Azad Jammu and Kashmir. **a** The inset shows the lithology of Lockhart Limestone (Yadgaar area), in the Upper Indus basins, **b** Fossils abundance and range chart

In the study area of Yadgaar section (Fig. 2), the lower contact of the Lockhart Limestone is observed as unconformable with Hangu Formation while the upper contact is marked erosionally unconformable with benthic forams rich Tethyan carbonates with shale microfacies, depicting intratidal lagoon/shore to open marine depositional circumstances in the basin (Khan et al. 2018b).

Materials and methods

Fieldwork

The fieldwork of two weeks includes formation identification, recognition of top and bottom, identifying outcrop microfacies, collection of 50 fresh representative rock samples at an interval of 1.5 m, and section measurement with the survey pole method, has been carried out. Initial lab work embraced rock cutting to the polishing of sample surfaces and then mounting on a slide with the help of epoxy resin was done which is followed by oven heating. Finally, a 2 mm thin slice of the mounted sample was cut again. Then, the careful grinding procedure is applied until the desired thickness (30 µm) and clarity are attained.

Petrography

For the petrographic evaluation of the Lockhart Limestone, we have selected the Yadgaar Section (Fig. 2) of Azad Jammu and Kashmir, and is studied under a polarized microscope (LEICA-DM 750P) to achieve a clear scheme of textural distribution, fossils assemblage, diagenetic features, modal mineralogical contents and its resultant behavior developed by post-diagenetic processes.

X-ray diffraction analysis (XRD)

Samples of shales are selected from the base and were sent for XRD analysis in the Centralized Resource Laboratory (CRL) at the University of Peshawar (Peshawar, Pakistan). The minerals identification through XRD experimentation on shale samples was carried out with JDX-3532 (made by JEOL Japan) X-ray diffractometer (XRD) with following specifications; Voltage = 20–40kv, Current 2.5–3.0 mA, Anode (X-rays) = CuKa (Wavelength = 1.5418 Å) and 2Theta-range = 0–600. Methods used to identify the minerals are of Goldsmith and Graf (1958) along with Goldsmith and Heard (1961). XRD analysis of Lockhart shales has been carried out to identify their mineralogical composition. Peak graphs (Fig. 8a–c) are identified with the MDI Jade 6 software.

Scanning electron microscopic study (SEM) for undersized fabric examination

The Lockhart Limestone samples are carefully studied under a Scanning electron microscope (SEM) of JEOL (Japan) at the Hi-Tech lab of the University of Azad Jammu and Kashmir, Muzaffarabad. First, these samples were polished and coated with thin aluminum foil (with the help of auto fine coater JEOL JFC-1600) to get the best image results. The aim of SEM is to obtain minerals information and correlate it with the XRD results to further confirm the mineralogical content of shales as well as the micro-diagenetic texture and cement type to evaluate the different stages of diagenesis in limestone (Fig. 10). Moreover, understanding the pore geometry and their abundance will reveal the reservoir properties of the Lockhart Limestone.

Results

Lithofacies of Lockhart Limestone

Lockhart Limestone of the Yadgaar Section in the UIB exhibits three lithofacies from base to top. In the base, light gray-colored calcareous pencil-like shales are present. Above this, a patch of banded portion, comprised of limestone intercalation with shales, is marked. The Middle-top portion of Lockhart Limestone contains light-colored medium bedded nodular limestone. Dispersed Carbonaceous Material (DCM) is marked throughout the formation. On the grounds of textural composition (Dunham 1962) and bioclasts type accounting for their abundance, microfacies of the Lockhart Limestone were identified and categorized. The attribute features of each facies will be discussed as follows:

Characteristics of microfacies in the Yadgaar section

Thin section study of the Lockhart Limestone encompasses analysis of grain sizes and sorting, which reveal fluctuation from finer particle sizes of lime mud to coarse-grained prevalence. Grain size ranges from 0.01 to 0.04 mm in the formation with an average value of 0.02 mm. Fine-grained micrite dominates the first microfacies (CMF-I), while the abundance of larger sized grains increases gradually towards the third microfacies (CMF-III). Furthermore, the petrographic studies reveal an abundance of dolomite crystals in some thin sections besides micrite with sometimes hematite, which acts as a filling material. The average ranges of micrite are 71%, bioclasts 12%, sparite 9.5% and carbonaceous material 2.6% in the Lockhart Limestone. Minor occurrences of dolomite, calcite, hematite, pyrite, framboidal pyrite and rutile in few specific samples are also observed. Cementing material is very fine-textured among variable micrite and dolomite grains.

First carbonate microfacies (CMF-I) is gray-colored mudstone found at the base of Lockhart Limestone. Micritized and dolomitized microfossils observed in this microfacies including green algae (*Beresellid* (Fig. 4d), *Donizellid* (Fig. 3a), *Spatangoid spine* (Fig. 3h) and *Uraloporella*), *Corallite* (Fig. 3e), *Discocyclina* (Fig. 4a), *Elphidiella* (Fig. 4g), *Fussilinidea* spp (Fig. 4f) and *Lockhartia haimei* (Davies 1927; Fig. 4e), *Lockhartia bermudezi* (Cole 1942: Fig. 4h), Fish remains and fish fossils (replaced by chalcedony and carbonaceous matter) were observed (Fig. 4b). Rutile (Fig. 3c), micritized bioclast (which is partly dolomitized; Fig. 3f) and pyrite (Fig. 4c) are also identified.

Second carbonate microfacies (CMF-II) is a light-colored, mudstone-wackestone-type slim rock body. A wide range of Paleocene benthic foraminifera's like *Assilina placentula* (Fig. 6d), *Asterocyclina* (Fig. 5h), *Cuvillerinella* spp (Fig. 5c), *Gastropods* with geopetal filling (Fig. 6b), (*Dascyclad)* Green algae (Fig. 5a), *Hemicyclammina sigali* (Fig. 6e), *Lockhartia* spp (Figs. 5e, 6a), *Melathrokerion valserinesis* (Fig. 6c), *Mesortolina subconcava, Orbitosiphon* (Fig. 6f), *Miscellanea miscella* (Fig. 5d), Ooids (Fig. 6g), *Quinqueloculina* (Fig. 5f, h), *Ranikothalia nuttalli* (Fig. 5g) and *Ranikothalia sindenesis* (Fig. 6d) were identified. Hematite and highly micritized fossils, replaced by carbonaceous matter (Fig. 5c) can also be observed.

The third carbonate microfacies (CMF-III) is a light grey colored wackestone-packstone, wide facies body. Micritic lime-mud sedimentation along with medium diagenetic grade cementation is found in this microfacies. Highly fossiliferous biota comprised of *Assilina laxispira* (Fig. 9b), *Assilina spinose* (Fig. 7a), *Coskinon* (Fig. 7g), Discocyclina (Fig. 7f), *Fusulinina bradyina* (Fig. 7c), *Gymnocodiaceae* (Green algaes) (Fig. 7e), *Lockhartia ramanae ten dam* (Fig. 6e), *Lockhartia daviesi ten dam*

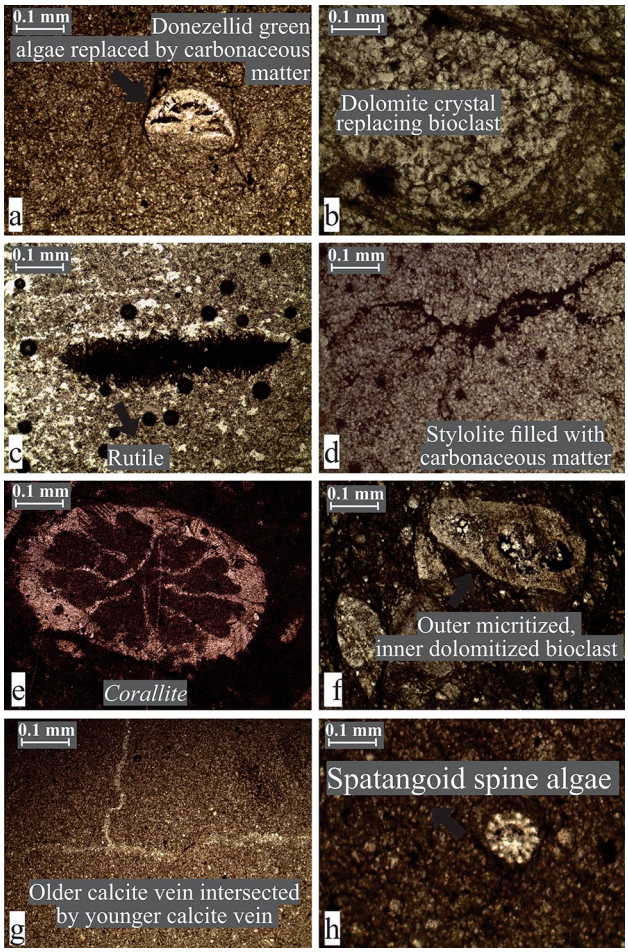

Fig. 3 Photomicrographs acquired from Lockhart Limestone (CMF-1) under plane-polarized light

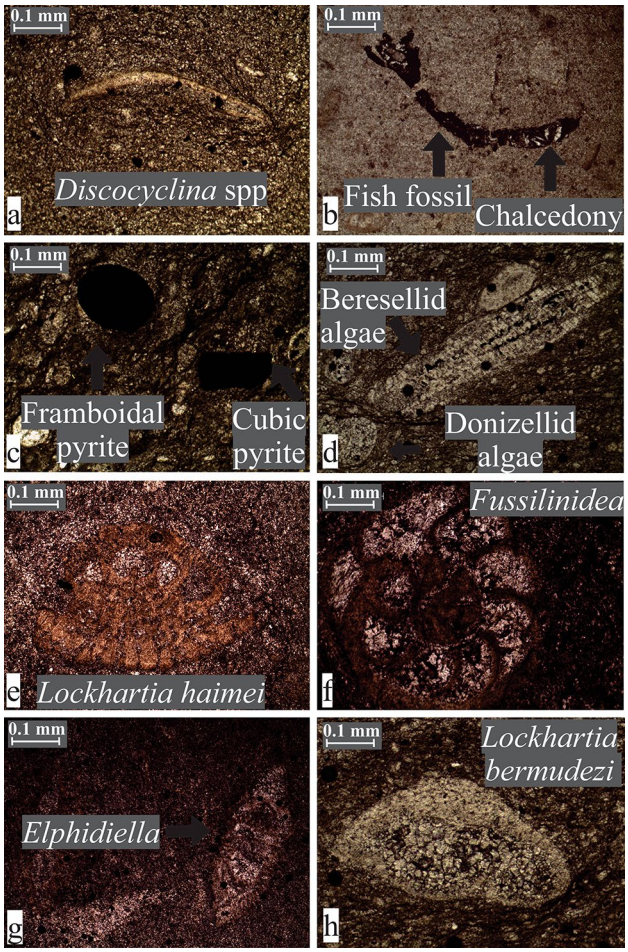

Fig. 4 Photomicrographs captured from mudstone and wackestone microfacies of Lockhart Limestone under plane-polarized light

(Ten Dam 1953; Fig. 6h), *Miscellanea miscella, Orbitolidea* (Fig. 7h), and *Quinqueloculina* is identified.

XRD analysis of shales

The detailed assessment of calcareous shales, which are observed with interbedded limestone, is evaluated to understand the mineralogical composition through XRD analysis (Fig. 8d). Results acquired from softwares such as: Jade and Origin pro were used for calculations, graph and diagram preparations. It reveals that calcite is a dominating carbonate mineral with the highest peaks (Fig. 9e). Quartz peaks were found as the second-highest, depicting its presence in a little amount and representing the silicate minerals. Secondary clay minerals like Kaolinite clay are present in a minor amount (Fig. 3a–c).

Scanning electron microscopic evaluations

Pencil-like shales are observed in the base of Lockhart Limestone and are selected for the SEM study. The first shale sample from the base (Fig. 10a) displayed fine-grained massive calcareous nature along with a small number of flakes belonging to the Ca-smectite clay. Ca-smectite started to decrease towards the second and third samples (Fig. 10b, c). Kaolinite clay can also be observed in the first two shale samples (Fig. 10a, b).

From the base towards the top, after the shale samples, we have selected nine limestone samples, three samples from each microfacies (base, middle and top), for the SEM analysis (Fig. 10d–k). As moving towards the first limestone microfacies (CMF-I; Fig. 10d–f), a sudden drop in clay minerals with the appearance of minor dolomite crystals, scattered in the calcite-dominated rock, is noted. In the middle of this microfacies clays completely vanished with a minor increase in dolomite crystals, is observed (Fig. 10e). Calcite abundance not only start to

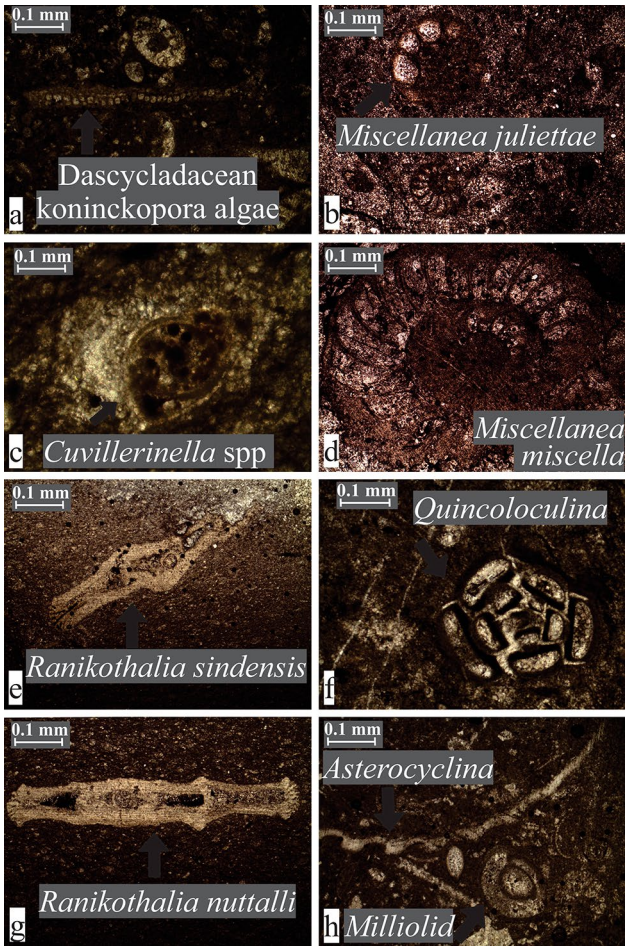

Fig. 5 Photomicrographs taken wackestone microfacies of Lockhart Limestone (CMF-2) under plane-polarized light

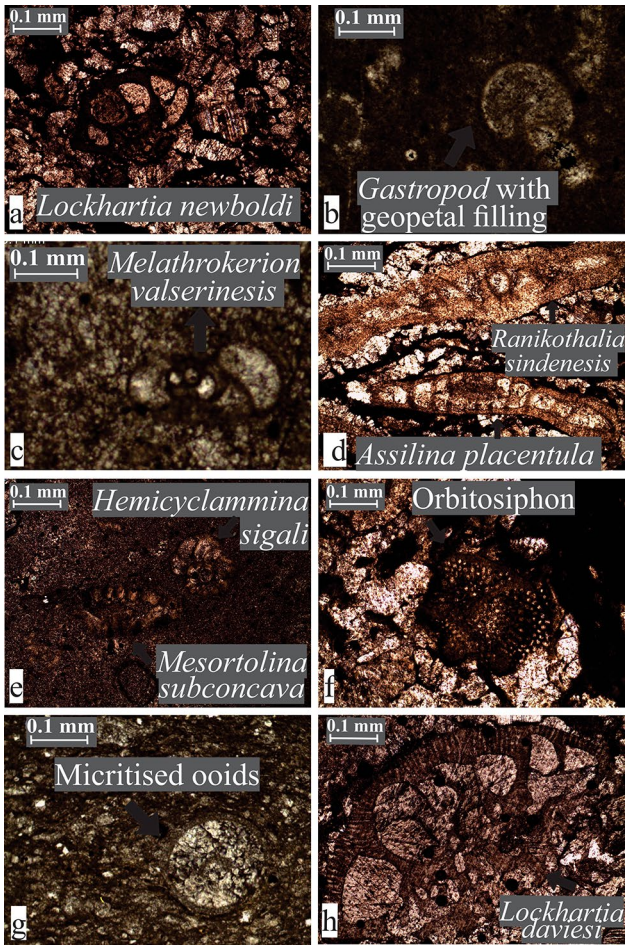

Fig. 6 Photomicrographs captured from wackestone and wackestone-packstone microfacies of Lockhart Limestone under plane-polarized light

increase but also the size of crystals becoming larger, with much more clear and overgrown crystals in the top portion of the first microfacies (Fig. 10f). Drusy and rim cement dominated in the lower to middle portion while rim cement appeared frequently at the top of this first microfacies.

Blocky cement is spotted in the base and top portion of the relatively coarse-grained second microfacies (CMF-II; Fig. 10g, i) along with the restricted occurrence of the rim cement in the center and granular cement at the base of this microfacies (Fig. 10g, h). A minor presence of dolomite is also noted near the top of the second microfacies (Fig. 10i).

The third microfacies (CMF-III) illustrated much coarser calcite crystals with the dominance of rim cement throughout the microfacies. However, drusy and blocky cement are also spotted in the lower portion along with a minor clay matrix and fibrous column of calcite at the top portion of the third microfacies (Fig. 10j, k).

Physical reservoir properties

A comprehensive study through image threshold enhancement technique in ImageJ software revealed pore spaces and their type in Lockhart Limestone (Fig. 5).

Porosity

The average porosity of CMF-I is 7% (Fig. 9a, b), while CMF-II illustrated some highest values of 16% in the second microfacies (Fig. 9c, d). The average value of porosity in the third microfacies (CMF-III) is 10% (Fig. 9e). CMF-II depicted the highest average value among all three microfacies, while the mean porosity value of the formation is calculated as 11%.

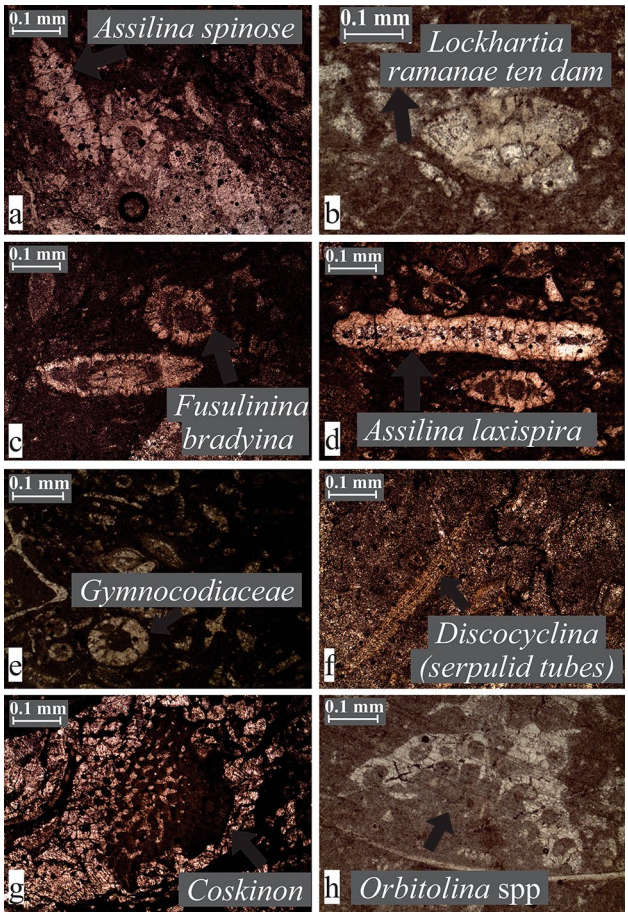

Fig. 7 Photomicrographs acquired from wacke–packstone microfacies of Lockhart Limestone (CMF-3) under plane-polarized light

Pore space portrayal permeability

As moving above from the base of the first microfacies (CMF-I), vuggy type porosity is dominantly observed, while, shelter (Fig. 9a), channel and fenestral types were also observed. Fenestral-type porosity is dominant in the middle of this microfacies (Fig. 9b).

As moving toward the CMF-II, an increase in porosity percentage has been revealed. This microfacies displays a dominant presence of channel and fracture (Fig. 9c) type porosities, commonly observed immediately around the medium to large-sized fossils (Fig. 9d) with few vuggy types at other places, respectively. CMF-III depicted fracture and moldic-type porosities often present immediately around the medium to large-sized fossils in the base. Vuggy type characterizes middle to top of the formation (Fig. 9e).

Discussion

The genesis of formational physical characteristics is subdued by the depositional environment and diagenesis (Li et al. 2021; Yang et al. 2018), which are observed and evaluated in the Lockhart Limestone. Depositional environment controls the initial petrological characteristics of microfacies, leading to the influence of the diagenetic process (Wang et al. 2020) resulting in porosity fluctuations (Bell et al. 2018).

The potential reservoir deposits of Lockhart Limestone dominantly fall in the Bio-micrite under Folk's classification (Folk 1965). However, variations were marked when this limestone was classified under Dunham's classification (Dunham 1962). It reveals mudstone, mudstone–wackestone and wackestone–packstone types. The carbonate platform microfacies in the study area were recognized by their specified occupancy in the toe of slope, slope and shelf areas. First carbonate microfacies (CMF-I) is a mudstone type narrow facies tract, representing its depositional site in minimal oxygenated deep and steeper slope site with water depth ranges from 200 to 300 m (Fig. 11). Sedimentation in this microfacies represents fine-grained micritic carbonate which is dolomitized and prone to high diagenetic alterations lately. This microfacies is equivalent to the FZ3 Toe of slope apron microfacies of Flugel (2010).

Second carbonate microfacies (CMF-II) is unlade along the nearly vertical slope of the platform margin with uneven grain sizes. This microfacies is equivalent to the FZ4 slope microfacies of Flugel (2010). The third carbonate microfacies (CMF-III) is deposited in a few meters' depths in shelf area with poor connectivity alongside the open ocean, resulting in fluctuated temperature and salinity range inside the euphotic zone. This microfacies is equivalent to the FZ8 Platform interior-restricted marine microfacies of Flugel (2010).

Sedimentary habitat and rock attribute

Estimation of rock components is carried out through petrographic studies. The micrite constitutes an average of 71% of the Lockhart Limestone, which clearly indicates the rock's nature as fine-grained micrite. However, the absence of sharp intragranular contact and pitted microspar crystals indicates the post-depositional deformation prone to rock formation (Munnecke and Samtleben 1996). Petrographic studies revealed low magnesium calcite (Fig. 3a, g) dominates in the thin sections which directed about the nature of the ocean as calcite sea. Fitted texture in the low magnesium calcite rock body (in CMF-I) indicates low depositional porosity and permeability as well as deposition in calm marine, meteoric water conditions (Hashim and Kaczmarek

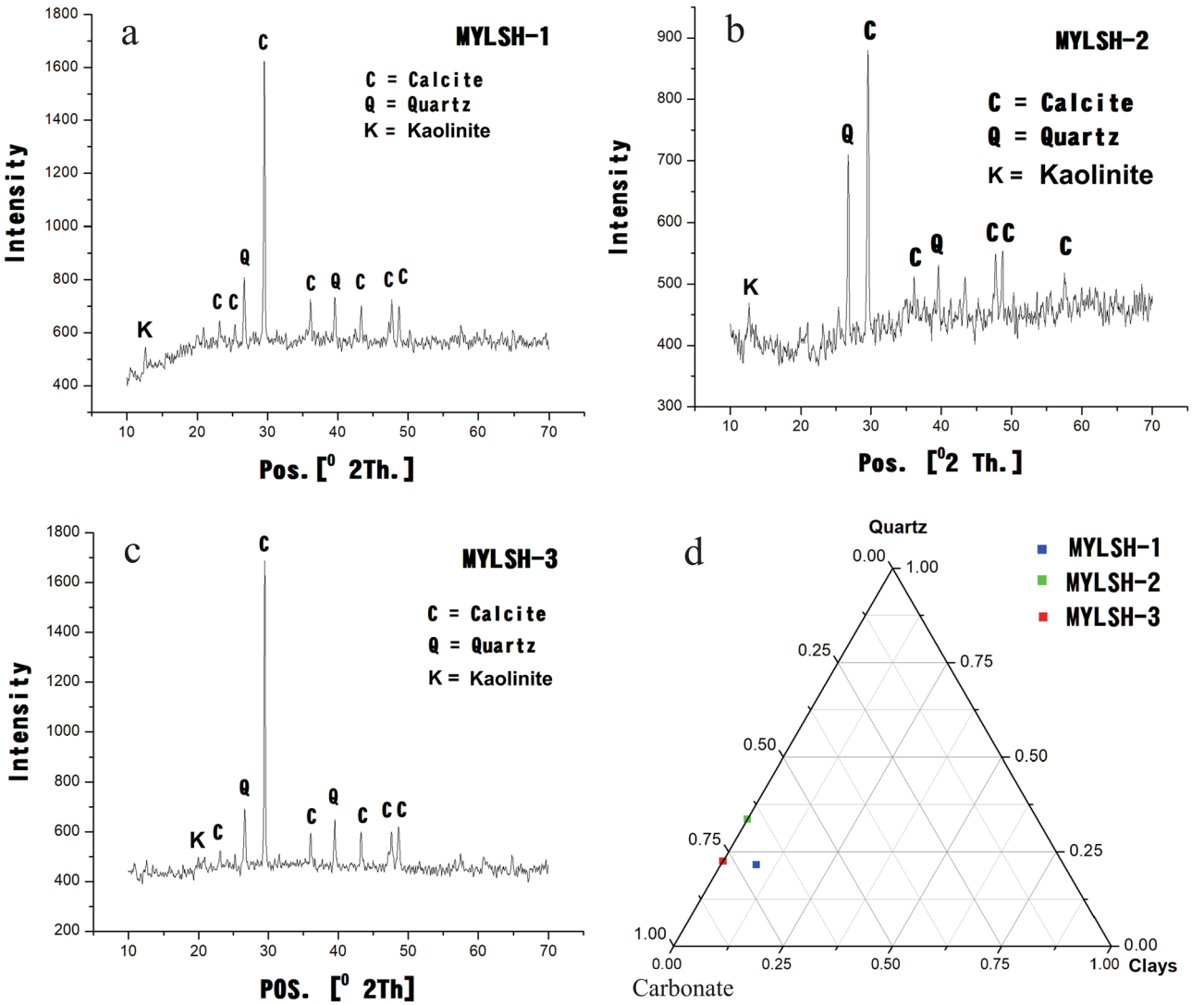

Fig. 8 Images **a**–**c** display the illustration of XRD peak graph results from the three shale samples from the base of Lockhart Limestone: **d** image displays XRD samples plotted on a triangular diagram of Carbonate, Quartz and Clay

2019). Dissolution of salt through meteoric water may create initial porosity in Lockhart Limestone. Low magnesium calcite may be formed fundamentally without bearing any effect of recrystallization (Huang et al. 2019).

The average foraminiferal fossils type content is 12%, depicting shallow marine shelf deposition on a carbonate platform. Dispersed carbonaceous material (DCM) has been observed throughout the Lockhart Limestone with an average of 7%. DCM indicates a reducing environment and a near source of vegetation as well as the presence of diagenesis (Azizi et al. 2014). The carbonaceous matter is highly volatile to migration and their presence along bioclasts (Fig. 3a) and stylolite (Fig. 3d) are observed in the Lockhart Limestone of the studied area. This is probably of secondary redeposited nature in the 108–164ºC temperature range (Patnaik et al. 2016).

Lockhart Limestone also comprised of dolomite patches found unevenly distributed throughout the formation (Fig. 3b). The presence of dolomitization in minor amounts is associated with the formation's fluid hydrology, caused by mixing of shelf water with magnesium-rich ocean water (Newport 2015). Petrographic studies revealed the occurrence of calcite veins in the Lockhart Limestone (Fig. 3g). Calcite vein formed when calcium-rich solution percolates through a tectonic related fracture, indicating the pressure and diagenetic effect on the formation (Cabral et al. 2019). Rutile in the Lockhart Limestone (Fig. 3c) represents detrital occurrence, derived from intra-basinal igneous or metamorphic rock.

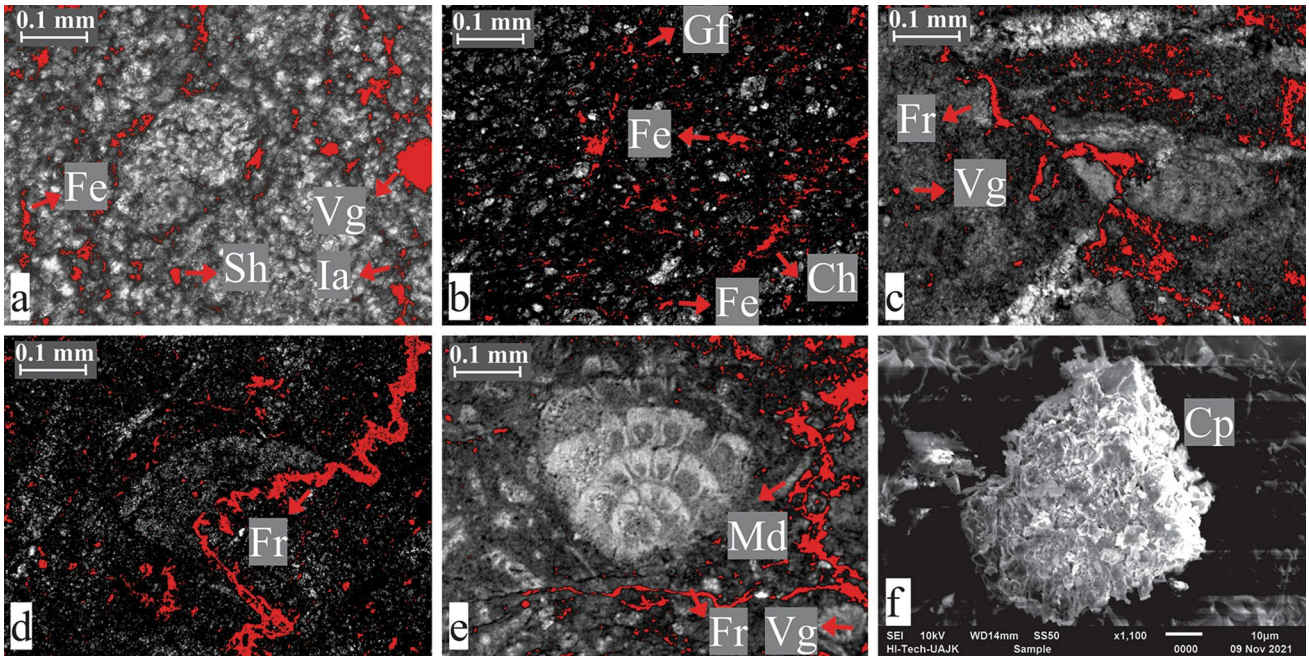

Fig. 9 Photomicrographs captured from thin section samples of Lockhart Limestone (under plane-polarized light except for f, which is an SEM image). **a**, **b** snapshot from CMF-I illustrates different types of porosities including Fenestral, Shelter, Intraparticle, Vuggy, Channel and Growth framework: **c**, **d** image reflects Fracture and Vuggy type of porosities with microfossil in CMF-II; **e** photomicrograph depicts Moldic, Fracture and Vuggy types of porosities in CMF-III; (f) SEM image illustrated cubic pyrite grains in CMF-I. Abbreviations are shown in Figs are: *Cp* Cubic pyrite and porosities types are *Fe* fenestral, *Sh* shelter, *Ia* intraparticle, *Vg* vuggy, *Fe* fenestral, *Gf* growth framework, *Ch* channel, *Fr* fracture, *Md* moldic-type porosities

Pyrite and framboidal pyrite

In the Lockhart Limestone besides carbonaceous material, cubic pyrite and framboidal pyrite (Fig. 4c) are also present. The presence of pyrite indicates decaying organic matter representing syngenetic reducing conditions along with early diagenesis (Dill et al. 2007). It occurs in the ocean where the water starts to transgress in the area and react with pyrite resulting in the formation of hematite. In the deep biosphere, the formation of sulfides (FeS and H_2S) is triggered by sulfate-reducing bacteria (SRB) leading to the formation of pyrite (FeS_2) in between 4 and 28 °C. Basic elements for FeS and H_2S were derived from Hydrothermal solutions and carbonaceous matter, respectively (Thiel et al. 2019). Relatively deeper microfacies of Lockhart Limestone in the Ceno-Tethys Ocean display the presence of pyrite in the Yadgaar section. Duverger et al. (2020) postulate that if the deposits were further prone to diagenesis for a long time, it may lead to the evolution of cubic pyrite into framboidal pyrite.

The framboidal pyrite (Fig. 10l) indicates anoxic and supersaturated mono-sulfide conditions and the occurrence of carbonaceous matter of simple alkane grade of hydrocarbon (Merinero et al. 2019). Rickard (2019) suggested that the framboidal pyrite abundance depicted anoxic to redox paleo-conditions in that portion of the rock. In the lower part of Lockhart Limestone, the first microfacies (CMF-I) shows the presence of framboidal pyrite. It is then observed in a minute amount in the lower second microfacies (CMF-II) which suddenly vanished in the middle-top portion of the formation. The formation of framboidal pyrite is directly associated with the hydrothermal fluids which percolate during diagenesis (Hayes et al. 2015). The evolution of framboidal pyrite in Lockhart Limestone may happen from the underlying Hangu Formation's (hosting laterite ore; Qasim et al. (2020) diagenetic fluids. They arise with dissolved pyrite and percolate through Lockhart Limestone during diagenesis, which facilitates hydrothermal alteration. This process leads to the formation of framboidal pyrite in the lower portion of the section. The original structure of framboidal pyrite may be affected due to various diagenetic outcomes like dissolution and recrystallization (Rajabpour et al. 2017). Framboidal pyrite smaller than 13 µm diameter belongs to syngenetic origin with the exogenic environment (Wilkin and Arthur 2001), while greater than 18 µm depicted diagenetic origin with the dysoxic environment (Wei et al. 2015). Lockhart Limestone displays framboidal pyrite with a size range between 150 and 200 µm.

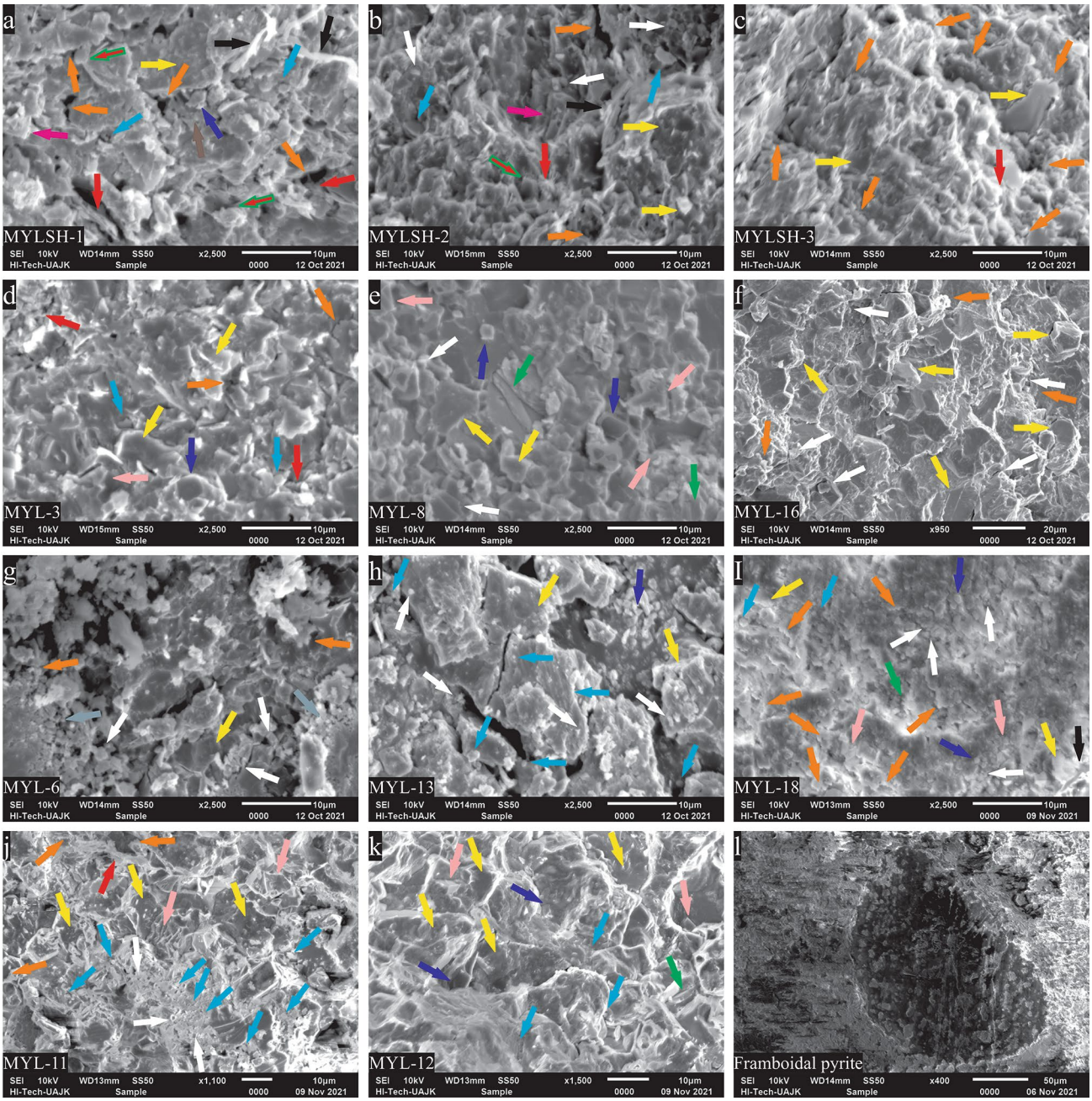

Fig. 10 SEM image of shales and limestone samples from Lockhart Limestone. Yellow arrows indicate calcite crystals, red arrows show ca-smectite clay matrix, red arrows with green outlines indicate kaolinite clay, indigo blue arrows depicted dolomite crystals, brown arrows show drusy cement, white arrows show blocky cement, sky blue arrows show rim cement of Prothero and Schwab (2014). However, green arrows show a fibrous column of calcite, light pink arrows showed mosaic (drusy) dolomite cement, silver arrows show granular cement, black arrows show radiaxial fibrous cement and the dark purple arrows show dog tooth calcite crystal of Flugel (2010)

Diagenetic influence on reservoir standards

Limestone reservoirs have great significance in the world's petroleum system. Porosity, permeability, fractures and diagenetic alteration plays key role in affecting the reservoir standards, globally (Li et al. 2021). During the tectonic uplifting and frequent weathering conditions, carbonate rocks are often prone to epidiagenesis processes which in turn proved to be very progressive toward the improvements in reservoir characteristics (Baiyegunhi et al. 2017). Lockhart Limestone may display epidiagenetic developments where primary depositional porosity is prone to reduction and later on leads to the

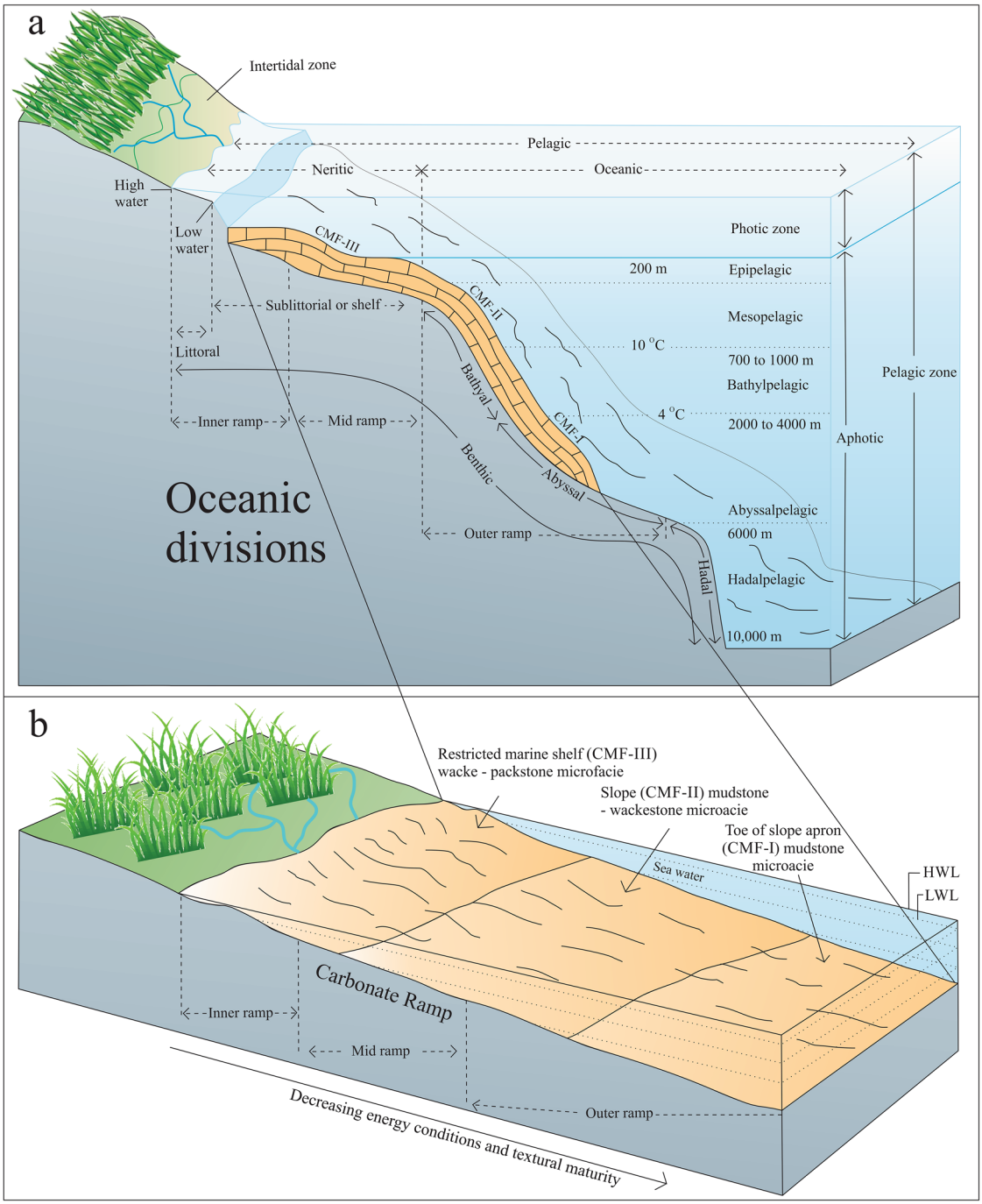

Fig. 11 **a** Three-dimensional model of a carbonate continental shelf sedimentary setting, representing the sedimentary conditions of the Upper Indus Basin; **b** Sectional model of inner, middle and outer carbonate shelf and representative deposits

development of secondary porosity in response to fracturing, dolomitization, etc. The physical reservoir nature was affected when a formation's diagenetic fluids move in pore spaces after undergoing burial due to the rise in temperature and pressure (Fan et al. 2016). Dolomitization, compaction, replacement, micritization, dissolution and cementation were observed as diagenetic factors which reduce the initial porosity and create the secondary porosity in the Lockhart Limestone. Clear signs related to partly micritization of bioclasts indicate diagenesis in the rock (Fig. 3a; 4a).

Relationship between dolomitization and reservoir

Lockhart Limestone possesses patches of dolomite and a minor amount of smectite in the formation. The selective patches of dolomite were thought to be produced by a local abundance of Mg/Ca ratio from non-evaporitic fluids at the low temperature accompanied by sulfate reduction by bacterial activities (Kaczmarek and Sibley 2011). Moreover, carbonaceous matter from a nearby source satisfies the supply of required carbon through the dissolution process for dolomitization. Mg^{2+} is mainly released during the conversion of smectite into illite at 50–60 °C (Chatalov 2018; Milliken 2003).

However, a strong explanation for this selective dolomitization contradicts the older theory, because the intensity of dolomitization gradually increases from the base towards the middle of the section, which suddenly vanished at the middle to top portion. It may depict oceanic transgression (Dill et al. 2007). It also indicates the low diagenetic compaction in the lower portion of the Lockhart Limestone but in the late time at the upper portion, high compaction seizes the mobility of the fluids which are responsible for the dolomitization processes (Figs. 4h; 5f; 6g). This is because of increasing post-collision folding faulting processes in the region between India and Eurasia followed by Himalayan orogenic development with the presence of the study area in the core of HKS, near to the hinterland region.

The petrographic character indicates that the mixture of fluids drives carrying Mg^{2+} ions in a coastal area, resulting in the distribution of small to medium-sized dolomite strata. Post-sedimentary event during late diagenesis produces these dolomite patches in the Lockhart Limestone. However, under deep burial and late diagenesis, early pore spaces are squeezed out and the influx of fluids carrying Mg^{2+} ions is reduced considerably. This may cause slowing down the dolomitization process hence we found only a small dolomitized portion in the microfacies (Haldar 2014). That is why dolomite crystal sizes were not fully developed due to the cut-off of the fluids supplies for a long time, in Lockhart Limestone. However, a transformation from microcrystalline towards macrocrystalline texture has been noted in dolomitized portions of the Yadgaar section (Fig. 3b, f).

Effect of dissolution and compaction on reservoir

Dissolution occurred in Lockhart Limestone by acidic and high-temperature fluids, which may increase void spectrum as well as cause cracking of the grains in carbonate strata re-creating much higher secondary porosity (Fig. 9d). Most of the drusy calcite cement is transformed into granular cement. Prothero and Schwab (2014) pointed similar type of action as neomorphism under burial.

In contrast to sandstone, carbonate strata can prone to diagenesis at a very shallow depth of < 1 km in which clay content, mineralogy, grain size and packing play an important role in the physical compaction of the rock in depth. In Lockhart Limestone, initial porosity is reduced up to 30% due to mineralogical suitability (Chemical compaction), while < 1% reduction can be observed through mechanical compaction and cementation. Therefore, under pressure, rearrangement of the particle framework took place which considerably affect the porosity by close packing in the Lockhart Limestone (Baques et al. 2020).

A porosity value of 11% in the Yadgaar section may be the result of high-stress level, developed in the core of the Hazara Kashmir Syntaxial bend (HKS). This indicates that the intensity of tectonic folding has a direct relationship with diagenesis as well as reservoir characteristics. On behalf of the direct relationship between porosity and permeability and the presence of channels and fracture type porosities (Fig. 9d, e), we may validate the existence of fair permeability in the Lockhart Limestone.

SEM analysis of shales, cement and effect of cementation on reservoir

Lockhart Limestone is comprised of pencil-like shales at the base. Davies et al. (2020) suggested that under low-temperature tectonic compression, the growth of pencil-shaped shales developed perpendicular to maximum stress and parallel to the minimum stress side. Minerals attempt to escape under the tectonic stress and with the help of pressure solutioning help to build cleavage resulting in a pencil-like shape.

Kaolinite and Ca-smectite as clay minerals are identified in the shales (Figs. 8a–c; 11a–c). Ca-smectite is formed by the dissolution and weathering of mica and feldspar under an epidiagenetic environment (Ekinci et al. 2018), however, clay minerals may be locally replaced by calcite crystals, lately (Baiyegunhi et al. 2017). Kaolinite in the shales present in the base of Lockhart Limestone may come from the underlying Hangu Formation. Hangu Formation comprised bauxite deposits in the Yadgaar Section (Bilal et al. 2022). These deposits consist of gibbsite which has been altered partly into kaolinite which may have been transported to the nearby shales of Lockhart Limestone (Baig and Munir 2007). This can further have supported by the high presence of Kaolinite in the sample found in the base and its concentration is reduced while moving upward in the section (Fig. 10a, b). Drusy and rim cement were observed in shales with minor blocky cement along with a negligible amount of dogtooth calcite crystal (Fig. 10a–c). Dogtooth calcite crystal depicted local de-dolomitization when calcium ions abundance is restored and magnesium ions level drops (Chen et al. 2006). Drusy and drusy dolomite types

of cement are spotted in the Lockhart Limestone (Fig. 10). Drusy cement indicates high percolation of hot brine diagenetic fluids originated from compressional tectonics which in turn alter the drusy calcite into drusy dolomite cement (Mansurbeg et al. 2021).

Eogenetic is the first substage of post-depositional diagenesis which is encompassed by the low porosity, evaporates or minerals precipitation along with channel and vuggy porosity (Vacher and Mylroie 2002). The first microfacies (CMF-I) from Lockhart Limestone depicted the lowest porosity along with the presence of minerals that may prone to the Eogenetic stage. Drusy to blocky cement depicted first to the second generation of cementing material present in this petrofacies.

The mesogenetic stage is the second sub-step of post-depositional diagenesis indicated by the presence of mosaic coarsely crystalline calcite crystals along with relatively high porosity. Telogenetic stages also depicted common fractures among the carbonate rock formations along with the fracture, channel and vuggy type porosities (Mylroie and Mylroie 2013). Both the second and third stages are clearly traced in the second microfacies (CMF-II) by the presence of large calcite crystals (Fig. 10h) along with high porosity values as well as with the occurrence of fractures (Fig. 9d), channels and vuggy (Fig. 9c) type porosities. Moreover, both rim and drusy cement (Fig. 10h, i) dominated in the petrofacies (CMF-II) indicating third-second generation cementing material. The third microfacies (CMF-III) demonstrates large angular calcite crystals along with the rim and blocky cement (Fig. 10j, k) may indicate the telogenetic stage in the microfacies.

Relationship of replacement and micritization with reservoir

Replacement and micritization effects dominate the bioclast and micrite material in the Lockhart Limestone of the Yadgaar Section. Micritized bioclasts sometimes were found to be further replaced by carbonaceous material (Fig. 3a). Geologists worked on in situ field experimentations that involves single crystal or grains to understand the kinetics of carbonate rocks (Putnis 2018). These experiments indicate that the event of mineral replacement results in porosity generation occurred during the inequilibrium mineral dissolution and precipitation stage (Minde et al. 2020). Dolomitization episodes on a small scale can be observed in the Lockhart Limestone with reshuffling caused in the initial porosity reduction in one hand, and creating intergranular porosity between euhedral dolomite crystals at the other hand (Fig. 3b). Moreover, the replacement process in dolomitization includes the transformation of crystals from anhedral to euhedral shape (Fig. 10). Mehmood et al. (2018) examined a similar process that was responsible for the creation of the intragranular porosity.

Due to the microbial activity, when the primary skeletal framework of carbonate alters into the finer cryptocrystalline texture (< 4 μm), then the process is called micritization. Bioclasts within the Lockhart Limestone were found half-fully micritized. They exhibit micritization intensity increases from the base towards the top (Figs. 3a; 4a). This may occur because of the less abundance of microbes in the anoxic environment which increases towards the top oxygenated environment. Even in some cases, bioclast was first micritized and then replaced by carbonaceous material (Fig. 3a). Micritic rock holds a much more valuable pore structure, illustrating initial porosity > 20%. However, it may prone to considerable reduction after diagenetic alterations. Lockhart Limestone exhibits 11% porosity in the Yadgaar section.

Control of microfacies on reservoir

Relationship between grains structure, particle composition and reservoir

Carbonate rocks of Lockhart Limestone mainly constitute fine-grained micrite with a reasonable amount of bioclasts and carbonaceous matter along with the little presence of sparite, calcite and hematite. The diameter of the pore throat and crystal shape has influenced the intercrystalline microporosity (Regnet et al. 2015) which in our case is narrow and well-packed. Mudstone microfacies in the base have relatively more packing due to finer particle size as compared to the other two microfacies. This is why CMF-I bears minimal porosity values amongst all three microfacies (Fig. 9a, b). In contrast, CMF-II in the middle has maximum-sized angular grains with larger pore throat sizes (Fig. 10g, h), along with some dolomite and bears the maximum porosity values among the microfacies, still after the diagenesis (Fig. 9c, d).

Relationship between stylolite and reservoir

Stylolites are the solution seams found parallel to the bedding plane. In Lockhart Limestone stylolites are often filled with carbonaceous matter (Fig. 3d). Distribution of stylolite differs in the Lockhart Limestone with much abundance in base and top portions of microfacies. However, a relatively low concentration in the middle portion has been noted. Under burial conditions and tectonic stresses, the pressure solutions that arise from the underlying Hangu Formation, were responsible to create wide stylolites. When compaction act on them, they may shrink and cause a reduction in the porosity of Lockhart Limestone. Movement of 0.1 mm can be observed in stylolite when they developed in bioclast (Fig. 10d). Moreover, stylolites may responsible to lower

the porosity by forming macroscopic diagenetic lamination. It may create barriers against calcifying fluids (Humphrey et al. 2019).

Effect of microfacies on pore evolution of reservoir

Lockhart Limestone of the Yadgaar Section is exposed to high temperature and pressure which brings about early metamorphism. It triggers diagenetic processes in the rocks which facilitates microscopic level changes. Secondary structures were the outcome of diagenesis. Compaction and cementation are found responsible footprints of porosity-reducing agents, while recrystallization and tectonic rapture implement positive effects on reservoir properties (Chen et al. 2016). Secondary structures, compaction, cementation and recrystallization are commonly observed in Lockhart Limestone.

Shallow marine carbonate platform microfacies indicate a high initial porosity range. Low amount of cement precipitation under early diagenesis caused an initial effect on reservoir properties. However, a rare amount of chalcedony (Fig. 4b) and chert grains indicates low temperature and diagenetic replacement. It also indicates sensitive changes in the physical and chemical properties of reservoir rock in the middle-late diagenesis (Li et al. 2021). Lockhart Limestone faces low cementation but high compaction and diagenetic conditions (Fig. 10).

CMF-I mudstone microfacies of Lockhart Limestone present at the base of the formation represent algal-dominant fine-grained lime mud. High grades of micritization alter the fossils completely (Fig. 4d, e). The presence of carbonaceous matter (Fig. 3a) and pyrite cubes (Fig. 4c) indicates an early stage of diagenesis in reducing conditions. In Lockhart Limestone, they probably came from solutions that carry soluble iron from the underlying sedimentary rock near the depositional site. However, pyritization can also occur from the decay of organic matter as well as by bacterial activity which can transform the sulfate ions (from pore water) into sulfide, which may result in the crystal growth of iron sulfide (Arnaud et al. 2020). Partly dolomitized and partly micritized (outer micritized and inner dolomitized) bioclasts can be observed in this microfacies (Fig. 3f). Therefore, all these indications help us to deduct about freshwater-associated diagenetic environment leading to the reduction in porosity (Regnet et al. 2015).

CMF-II mudstone–wackestone and CMF-III wackestone–packstone microfacies of Lockhart Limestone were relatively coarse-grained strata, fossils rich and ranging from *Dascycladacean* algae to some large microfossils like Ooids (Fig. 6g), *Gastropods* (Fig. 6b), *Lockhartia* spp (Fig. 6a, h), *Assilina* spp (Fig. 6d), *Miscellanea* juliettae (Hayward et al. 2021; Fig. 5b) *Miscellanea miscella* (Fig. 5d) and *Milliolids* (Fig. 5f, h). Dolomitization can also be observed in some parts. Calcite veins were also seen overlapping each other indicating two phases of hydraulic fracturing which later on filled with calcite. Second-generation blocky cement can also be observed (Fig. 10). It indicates the second phase of diagenesis (Flugel 2010). By calculating the average effective porosity of Lockhart Limestone as 11%, we can assume that the initial porosity of the formation is around 25% and the reduction from the initial porosity is possibly minimized up to 56%.

Depositional environment in response to the development of Ceno-Tethys Ocean

The movement of the Indian plate towards the north was the episodic combination of slow and rapid events that caused the uprising in the Ceno-Tethys Ocean margins (Pusok and stegman 2020). Deposition of Thanetian-aged Lockhart Limestone in the Indus Basin took place during the transgression of the Ceno-Tethys Ocean in the realm. Detailed study of petrofacies, devised on the textural base as well as variegated benthonic foraminifera revealed each of their depositional site along with the carbonate platform. Microfacies from Lockhart Limestone were categorized as CMF-I, CMF-II and CMF-III belonging to the toe of slope, slope and shelf areas, respectively. These microfacies are found equivalent to the FZ3, FZ4 and FZ8 microfacies of Flugel (2010).

CMF-I mudstone microfacies is composed of very fine-grained micritic limestone with a wide range of Paleocene foraminifers (listed in 4. a.1.). Benthic foraminifera and Ostracod indicate relatively deep and cold marine conditions (Stalder et al. 2015). Insitu *Beresellid* algae depicted low energy, normal marine and interior platform settings, forming low porosity micrite microfacies (Choh and Kirkland 2008). *Spatangoid spine* algae are surrounded by inhomogeneous allomicritic matrix material formed under the circumstances of an episodic storm on a carbonate platform. During the transgression of the Ceno-Tethys Ocean in Paleocene time, the deposition of Lockhart Limestone took place in the carbonate platform and the water level starts rising and the basal mudstone microfacies was deposited (Fig. 11). Its sedimentation occurred in a calm and low oxygenated water along with the wide range of fossils, depicting normal saline conditions under the water depth of 200–300 m. This microfacies resemble to the FZ3 toe of the slope apron microfacies of Flugel (2010). By integrating petrographic and SEM data, we may deduct precise depositional environment for the first microfacies along with the pyrite (Fig. 4c) and framboidal pyrite (Fig. 10l) grains. The anoxic environment is deduced in a relatively larger depth of carbonate platform which hosts the formation of pyrite when sulfate-reducing bacteria (SRB) convert the sulfide minerals into pyrite. Mudstone

microfacies deposited with the pyrite in the toe of the slope region along the Ceno-Tethys Ocean (Fig. 11).

As the transgression of marine water continued with the deposition of wackestone strata depicting relatively coarse-grained second microfacies (CMF-II) of Lockhart Limestone. A wide range of Paleocene fossils (listed in 4. a.1.) were found in this microfacies. In the micrite matrix, the appearance of the pyrite, hematite (Fig. 9d) and dolomite crystals have also been observed. The presence of calcareous fossils indicates a nearby photic zone from where they settled in the deeper ocean after their death (Fleisher and Lane 1999). Size variation of grains along with a high abundance of fossils indicates the depositional environment of this microfacies took place in the slope of the carbonate platform (Fig. 8). This microfacies resembles the FZ4 slope lithofacies of Flugel (2010).

The top portion of Lockhart Limestone (CMF-III) represents the light grey colored wackestone–packstone microfacies with some large-sized benthic foraminiferas (listed in 4.a.1.). Lockhart Limestone is marked as the Thanetian Paleocene age due to the appearance of zonal fossils like *Lockhartia haimei*, *Lockhartia daviesi ten dam* and *Miscellanea miscella* (Sameeni et al. 2013; Ten Dam 1953). Medium–large-sized fossils depicted variegated salinity and temperature, as well as high oxygenated water. Moreover, fluctuating grain sizes from medium-large size, indicate the presence of depositional settings in the tidal and euphotic zone (Fig. 8). This type of environment is generally found in the restricted marine platforms e.g., lagoon present at the backside of reefs or atolls with shallow depth up to only a few meters (Sun et al. 2019). The microfacies resemble the FZ8 interior platform rock facies of Flugel (2010). After the closing of the Ceno-Tethys Ocean, the tectonic stresses built in response to Himalayan Orogeny may cause a diagenetic impact on those deposits. On the basis of the above indications (discussed in 5.b.3), we conclude that three generations of cementing material are the product of three stages of diagenesis, respectively, i.e. Eogenetic stage results in drusy, mesogenetic phase generate blocky and telogenetic level produce rim cement. Thus, it is proposed that stages of diagenesis are directly proportional to the cement type in Lockhart Limestone.

Conclusion

The following conclusions are drawn on the basis of field, petrographic, SEM and XRD analysis:

Based on the petrographic study, the Lockhart Limestone is divided into three petrofacies namely mudstone, mudstone to wackestone and wackestone to Packstone. These facies are deposited in the Ceno-Tethys Ocean at the toe of the slope, slope and shelf areas of a carbonate platform, respectively. These facies are highly micritized, fossiliferous and calcareous in Yadgaar Section.

XRD and SEM analyses indicate that the shales of the Lockhart Limestone are highly calcareous and their deposition occurred along a relatively deeper part of the Ceno-Tethys Ocean.

The Lockhart Limestone contains pyrite and carbonaceous material which are syngenetically formed from the bacterial action and decay of organic matter. Initial porosity is considerably reduced after diagenetic effects like compaction, cementation and micritization. However, various factors like stylolite veins, fracturing, dolomitization and dissolution caused in the regeneration of the secondary porosity indicate the responsible process of epidiagenesis, which makes the rock characteristics fit to be a potential reservoir.

The Eogenetic substage of diagenesis is marked in CMF-I, mesogenetic and telogenetic in CMF-II while the telogenetic substage of diagenesis is spotted in CMF-III of Lockhart Limestone. Moreover, the three generations of cementing materials may also form under the circumstances of these three post-diagenetic sub-stages, respectively.

Deposition of the basal microfacies (CMF-I) took place in deoxygenated and relatively deep carbonate platform where sulfides are converted into pyrite by the action of sulfate-reducing bacteria (SRB). Lockhart Limestone is then prone to a long-time diagenetic condition that converts pyrite into framboidal pyrite. The restricted presence of both pyrites to the basal microfacies proved not only a diagenetic effect on the Thanetian strata but also inferred that CMF-I is deposited in the deepest portion of the Ceno-Tethys Ocean as compared to the second and third microfacies.

On the basis of typical abundant species like *Miscellanea miscella*, *Lockhartia daviesi ten dam* and *Lockhartia haimei*, the age of Lockhart Limestone is assigned as Thanetian Paleocene.

Supplementary Information The online version contains supplementary material available at https://doi.org/10.1007/s13146-022-00823-z.

Acknowledgements This study was financially supported by China-ASEAN Maritime Cooperation Fund Project (Grant No.12120100500017001) and National Natural Science Foundation of China (Grant No. 41972146).

Author contributions All authors contributed to the study conception and design. Material preparation, data collection and analysis were performed by AB, RY, FA, MSM, LY, MB and MF. The first draft of the manuscript was written by AB and all authors commented on previous versions of the manuscript. All authors read and approved the final manuscript. Conceptualization: AB and RY. Methodology: AB and FA. Formal analysis and investigation: AB, MB and MF. Writing—original draft preparation: AB. Writing—review and editing: AB and LY. Funding acquisition: RY and FA. Resources: AB and RY. Supervision: RY and MSM.

Data availability The data used to support the findings of the study are included within the article.

Declarations

Conflict of interest The authors have declared that no competing interests exist.

References

Afzal J, Williams M, Aldridge RJ (2009) Revised stratigraphy of the lower Cenozoic succession of the Indus Basin in Pakistan. J Micropalaeontol 28:7–23

Ahmed T, Mehboob S, Panni MSK, Yaseen A, Iltaf KH (2018) Foraminiferal biostratigraphy and microfacies analysis of the Paleocene (Thanetian) Lockhart limestone from Yadgar section, Muzzafarabad and Nammal Road section, Mianwali, Pakistan. In: 5th International Conference Earth Sciences Pakistan, Baragali Campus, pp 11–13

Ahsan N, Shah, MM (2017) Depositional setting and reservoir quality of the Lockhart Limestone (Lower Paleocene) in the Hazara-Kashmir Basin AAPG data search and discovery Article #90291. In: American Association of Petroleum Geologists, Annual Convention and Exhibition (Texas), p 2–5.

Arnaud D, Berg JS, Vincent B, François G, Sylvain B, Jennyfer M (2020) Mechanisms of pyrite formation promoted by sulfate-reducing bacteria in pure culture. Front Earth Sci 8:457. https://doi.org/10.3389/feart.2020.588310

Awais M, Ullah F, Khan N (2019) Investigation of reservoir characteristics, depositional setting and T–R sequences of the Lockhart Limestone of Meyal Oil Field, Pakistan: a petrophysical approach. J Petrol ExplorProd Technol 9:2511–2530

Azizi SHH, Shabestari GM, Khazaei A (2014) Petrography and geochemistry of pal-eoc limestones in Ching-dar syncline, Eastern Iran. Geosci Front 5(3):429–438

Baig MS, Munir MUH (2007) Foraminiferal biostratigraphy of Yadgar area, Muzaffarabad Azad Kashmir, Pakistan. 40

Baiyegunhi C, Liu K, Gwavava O (2017) Diagenesis and Reservoir properties of the Permian Ecca Group Sandstones and Mudrocks in the Eastern Cape Province South Africa. Minerals 7:88. https://doi.org/10.3390/min7060088

Baques V, Ukar E, Stephen E, Laubach S, Forstner R, Fall A (2020) Fracture, dissolution, and cementation events in Ordovician Carbonate Reservoirs, Tarim Basin, NW China. Geofluids 2020:1–28

Bell D, Kane IA, Ponten AS (2018) Spatial variability in depositional reservoir quality of deep-water channel-fill & lobe deposits. Mar Petrol Geol 98:97–115

Bilal A, Mughal MS, Janjuhah HT, Ali J, Niaz A, Kontakiotis G, Antonarakou A, Usman M, Hussain SA, Yang R (2022) Petrography and provenance of the Sub-Himalayan Kuldana Formation: implications for tectonic setting and Palaeoclimatic conditions. Minerals 12(7):794

Cabral FAA, Silveira ACD, Ramos GMS, Miranda TSD, Barbosa JA, Neumann VHDML (2019) Microfacies and diagenetic evolution of limestones of the upper part of Crato Fm, Araripe Basin, northeastern Brazil. Braz J Geol 49:1

Chatalov A (2018) Origin of fabric-selective dolomitization recognizable in the field: two case studies from Anisian carbonate rocks in the west Balkanides. Geologica Balcanica 47:43–60

Chen Q, Luo K, Hu K (2006) Discussion on the forming factors of dog-tooth crystal and stone coral in Furong cave, Chongqing China. Carbonates Evaporites 21:161–169

Chen Q, Liu QW, Wang S (2016) Study of diagenesis and pore evolution of Triassic Jialingjiang formation in Southern Puguang Gasfield. J Chem. https://doi.org/10.1155/2016/7328326

Choh SJ, Kirkland BL (2008) Sedimentologic role of in situ Beresellid algal colonies, Holder Formation (Upper Pennsylvanian), New Mexico, USA. Carbonates Evaporites 23(2):79–88

Cole WS (1942) Lockhartia in Cuba. J Paleontol 16(5):640–642

Davies LM (1927) The Ranikot Beds at Thal (North-West Frontier Provinces of India). Q J Geol Soc 83(1–5):260–290

Davies H, Blanco DF, Gürer D, Papeschi S, Rijsingen EV, Brizzi S, Pluymakers A (2020) Blog of the tectonics and structural geology (TS) Division of the EGU. https://blogs.egu.eu/divisions/ts/2020/08/07/features-from-the-field-pencil-cleavage

Dill HG, Wehner H, Kus J, Botz R, Berner Z, Stüben D, Al-Sayigh A (2007) The Eocene Rusayl Fm, Oman, carbonaceous rocks in calcareous shelf sediments: environment of deposition, alteration & H–C potential. Int J Coal Geol 72:89–123

Dunham RJ (1962) Classification of carbonate rocks according to depositional texture. Am Assoc Petrol Geol 1:108–121

Duverger A, Berg JS, Busigny V, Guyot F, Bernard S, Miot J (2020) Mechanisms of pyrite formation promoted by sulfate-reducing bacteria in Pure Culture. Front Earth Sci 8:457. https://doi.org/10.3389/feart.2020.588310

Ehsan M, Gu H, Akhtar MM, Abbasi SS, Ehsan U (2018) A geological study of reservoir formations and exploratory well depths statistical analysis in Sindh Province, Southern Lower Indus Basin Pakistan. Kuwait J Sci 45(2):84–93

Ekinci ŞB, Esenli F, Kadir S, Elliott W (2018) Genesis of smectite in siliciclastics and pyroclastics of the Eocene İslambeyli Formation in the Lalapaşa region, NW Thrace Turkey. Clay Miner 50(4):459–483. https://doi.org/10.1180/claymin.2015.050.4.04

Fan A, Wu X, Wang L, Zhang C, Guo J (2016) Diagenetic mineral transformation and reservoir physical properties in southwest Sulige gas field Ordos Basin. Nat Gas Geosci 27(07):1190–1201

Fleisher RL, Lane HR (1999) Treatise of petroleum geology/handbook of petroleum geology: Exploring for oil and gas traps. Chapter 17: Applied paleontology: American Association of Petroleum Geologists Bulletin

Flugel E (2010) Microfacies of carbonate rocks, analysis, interpretation and application. Springer-Verlag, Berlin, pp 1–921

Folk RL (1965) Some aspects or recrystallizaltion in ancient limenones. In: Pray LC, Murray RC (eds) Dolomitization and limestone diagenesis. SEPM Special Publication (13):14–48

Haldar SK, Josip T (2014) Chapter 5—sedimentary rocks. In: Haldar SK, Tišljar J (eds) Introduction to mineralogy and petrology. Elsevier, pp 121–212

Hasany ST, Saleem U (2012) An integrated subsurface geological and engineering study of Meyal Field, Potwar Plateau, Pakistan. American Association of Petroleum Geologists Search and Discovery article # 20151

Hashim MS, Kaczmarek SE (2019) A review of the nature and origin of limestone microporosity. Mar Pet Geol 107:527–554

Hayes TS, Cox DP, Piatak NM, Seal RR (2015) Sediment-hosted strata bound copper deposit model: US Geological Survey Scientific Investigations Report 2010-5070-M, 147. https://doi.org/10.3133/sir20105070M

Hayward BW, Le Coze, F, Vachard D, Gross O (2021) World Foraminifera Database. Miscellanea juliettae Leppig, 1988. Accessed at: http://www.marinespecies.org/foraminifera/aphia.php?p=taxdetails&id=1079157on2021-10-19

Huang H, Shanggui G, Niu L, Daniel B, Jörn P, Meng J, Ming C, Harry H, Roberts DC, Dong F (2019) Formation of authigenic low-magnesium calcite from sites SS296 and GC53 of the Gulf of Mexico. Minerals 9(4):251. https://doi.org/10.3390/min9040251

Humphrey E, Rivas EG, Koehn D, Bons PD, Neilson J, Martín JDM, Schoenherr J (2019) Stylolite-controlled diagenesis of a mudstone carbonate reservoir: a case study from the Zechstein_2_Carbonate (Central European Basin, NW Germany). Mar Pet Geol 109:88–107

Kaczmarek SE, Sibley DF (2011) On the evolution of dolomite stoichiometry and cation order during high-temperature synthesis experiments: an alternative model for the geochemical evolution of natural dolomites. Sed Geol 240:30–40

Khan IH, Clyde WC (2013) Lower Paleogene tectonostratigraphy of Balochistan: evidence for timetransgressive L Paleocene-E Eocene Uplift. Geosciences 3:466–501

Khan M, Khan MA, Shami BA (2018a) Microfacies analysis and diagenetic fabric of the Lockhart Limestone exposed near Taxila, Margalla Hill Range, Punjab Pakistan. Arab J Geosci 11:29. https://doi.org/10.1007/s12517-017-3367-4

Khan N, Naveed A, Mansoor A, Muhammad A, Naqib U (2018b) Hydrocarbon source rock potential evaluation of the Late Paleocene Patala Formation, Salt Range, Pakistan: Organic geochemical and palynofacies approach. J Earth Syst Sci 127:98

Khan N, Ahmad I, Ishaq M, Jan IU, Khan U, Awais M, Salam M, Khan B (2020) Reservoir Potential Evaluation of the Middle Paleocene Lockhart Limestone of the Kohat Basin, Pakistan: petrophysical analyses. Int J Econ Environ Geol 11(1):01–09

Li Y, Aiping F, Renchao Y, Yipu S, Nils L (2021) Sedimentary facies control on sandstone reservoir properties: a case study from the permian Shanxi Formation in the southern Ordos basin, central China. Mar Pet Geol 129:105083

Mansurbeg H, Alsuwaidi M, Dong S, Shahrokhi S, Morad S (2021) Origin of drusy dolomite cement in Permo-Triassic Dolostones, Northern UAE. Water 13:1908

Mehmood M, Yaseen M, Khan EU (2018) Dolomite and dolomitization model—a short review. Int J Hydrogen Energy 2(5):549–553

Merinero R, Ortega L, Lunar R, Piña R, Cárdenes V (2019) Framboidal chalcopyrite and bornite constrain redox conditions during formation of their host rocks in the copper stratabound mineralization of Picachos, north-central Chile. Ore Geol Rev. https://doi.org/10.1016/j.oregeorev.2019.103037

Metcalfe I (2021) Multiple Tethyan ocean basins and orogenic belts in Asia. Gondwana Res. https://doi.org/10.1016/j.gr.2021.01.012 (**ISSN 1342-937X**)

Milliken KL (2003) Late diagenesis and mass transfer in sandstone–shale sequences. In: Mackenzie FT (ed) Sediments, diagenesis, and sedimentary rocks. Treatise on geochemistry, vol 7. Elsevier-Pergamon, Oxford, pp 159–190

Minde MW, Udo Z, Madland MV, Korsnes RI, Schulz B, Gilbricht S (2020) Mineral replacement in long-term flooded porous carbonate rocks. Geochim Cosmochim Acta 268:485–508

Munnecke A, Samtleben C (1996) The formation of micritic limestones and the development of limestone-marl alternations in the Silurian of Gotland. Sweden Facies 34:159–176

Mylroie J, Mylroie J (2013) Telogenetic limestones and Island Karst. Springer. https://doi.org/10.1007/978-94-007-5016-6_17

Naeem M, Sadiq RAB, Anwar M, Khalid P (2014) Mechanical properties and petrographic characteristics of Margala Hill limestone and Lockhart limestone of Rumli area Islamabad Pakistan. Acta Geod Geoph 49:441–454

Nawaz M, Ub N, Bukhari SAA, Khan S (2015) Petrophysical analysis of Lockhart Limestone with porosity and thickness correlation of exposed Lockhart Limestone at Nathia Gali with subsurface Lockhart Limestone of Chanda deep-01 well in Upper Indus basin. J Himal Earth Sci 48:59–63

Newport RJ (2015) Controls on Dolomitization of Upper Cretaceous Strata of North Africa and Western Mediterranean. The University of Manchester (United Kingdom)

Patnaik S, Chakrabarti K, Pradhan A (2016) Petrographic charaterisation of carbonaceous matter in brecciated limestone at Kanchankayi area, Yaadgir district, Karnataka: Genetic implications for uranium mineralisation. J Appl Geochem 18:119–124

Prothero DR, Schwab F (2014) Sedimentary Geology—an introduction to sedminentary rocks and stratigraphy. W.H Freeman and Company, p 593

Pusok A, Stegman D (2020) The convergence history of India–Eurasia records multiple subduction dynamics processes. Sci Adv 6:19. https://doi.org/10.1126/sciadv.aaz8681

Putnis A (2018) Mineral replacement reactions. In: Oelkers EH, Schott J (eds) Thermodynamics and kinetics of water-rock interaction. De Gruyter, Berlin, Boston, pp 87–124

Qasim M, Ding L, Khan A, Baral U, Jadoon I, Umar M, Imran M (2020) Provenance of the Hangu Formation, Lesser Himalaya, Pakistan: insight from the detrital zircon U-Pb dating and spinel geochemistry. Palaeoworld 29:729–743

Qureshi MA, Ghazi S, Riaz M (2021) Geo-seismic model for petroleum plays an assessment of the Zamzama area, Southern Indus Basin, Pakistan. J Petrol Explor Prod Technol 11:33–44

Rajabpour S, Abedini A, Alipour S, Lehmann B, Jiang SY (2017) Geology and geochemistry of the sediment-hosted Cheshmeh-Konan redbed-type copper deposit NW Iran. Ore Geol Rev 86:154–171

Regnet JB, Robion P, David C, Fortin J, Brigaud Yven B (2015) Acoustic and reservoir properties of microporous carbonate rocks: implication of micrite particle size and morphology. J Geophys Res Solid Earth 120:790–811

Rickard D (2019) Sedimentary pyrite framboid size-frequency distributions: a meta-analysis. Palaeogeogr Palaeoclimatol Palaeoecol 522:62–75

Sameeni S, Haneef M, Shabbir F, Ahsan N, Ahmad N (2013) Biostratigraphic studies of Lockhart limestone, Changlagali area, Nathiagali-Murree road, Hazara, northern Pakistan. Sci Int (lahore) 25:543–550

Shah SMI (2009) Stratigraphy of Pakistan. Geol Surv Pak Memoir 22:1–381

Shah AA, Manan NA, Binti ANA, Catur C, Navakanesh MB, Malik JN (2020) Formation, rotation, and present-day configuration of Kashmir and Peshawar Basins in NW Himalaya. Front Earth Sci 8:441. https://doi.org/10.3389/feart.2020.569771

Stalder C, Vertino A, Rosso A, Rüggeberg A, Pirkenseer C, Spangenberg JE, SpezzaferriS CO, Rappo S, Hajdas I (2015) Microfossils, a key to unravel cold-water carbonate mound evolution through time: evidence from Eastern Alboran Sea. PLoS ONE 10(10):e0140223. https://doi.org/10.1371/journal.pone.0140223

Sun C, Hu M, Hu Z (2019) Sedimentary facies and sequence stratigraphy in the Lower Triassic Jialingjiang Formation, Sichuan Basin, China. J Petrol Explor Prod Technol 9:837–847

Ten Dam A (1953) Two new species of the foraminiferal genus lockhartia from Turkey. Türkiye Jeoloji Bülteni 4(1):84–98

Thiel J, James M, Byrne A, Kappler BS, Pester M (2019) Pyrite formation from FeS and H2S is mediated through microbial redox activity. PNAS 116(14):6897–6902

Tian X, Shi Z, Yin G, Wang Y, Tan Q (2017) Carbonate diagenetic products and processes from various diagenetic environments in Permian paleokarst reservoirs: a case study of the limestone strata of Maokou formation in Sichuan Basin South China. Carbonates Evaporites 32:215–230

Vacher H, Mylroie J (2002) Eogenetic Karst from the perspective of an equivalent porous medium. Carbonates Evaporites 17:182–196

Wang JJ, Wu SH, Li Q, Xiao SM (2020) Controls of diagenetic alteration on the reservoir quality of tight sandstone reservoirs in the Triassic Yanchang formation of the Ordos Basin China. J Asian Earth Sci 200:104472. https://doi.org/10.1016/j.jseaes.2020.104472

Wei H, Thomas J, Algeo H, Yu JW, Chuan G, Guo S (2015) Episodic euxinia in the Changhsingian (late Permian) of South China: evidence from framboidal pyrite and geochemical data. Sed Geol 319:78–97

Wilkin RT, Arthur MA (2001) Variations in pyrite texture, sulfur isotope composition, and iron systematics in the Black Sea: evidence for Late Pleistocene to Holocene excursions of the O2–H2S redox transition. Geochim Cosmochim Acta 65:1399–1416

Wilson JL (1975) Characteristics of carbonate platform margins. Am Assoc Petrol Geol Bull 58:810–824

Xia LW, Cao J, Wang M (2019) A review of carbonates as hydrocarbon source rocks: basic geochemistry and oil–gas generation. Pet Sci 16:713–728

Xiao D, Tan XC, Shan SJ (2014) The restoration of paleokarst geomorphology of Middle Permian Maokou formation and Its petroleum geological significance in Southern Sichuan Basin. Acta Geol Sin 88(10):1992–2002

Yang LI, Zhijiang KANG, Zhaojie XU, Zheng S (2018) Theories and practices of carbonate reservoirs development in China. Pet Explor Dev 45(4):712–722

Yu J, Zheng M, Li J, Wu X, Guo Q (2018) Resource potential, exploration prospects, and favourable direction for natural gas in deep formations in China. J Nat Gas Geosci 3:311–320

Zhu JC, Zou CN, Feng YL (2020) Distribution and controls of petroliferous plays in subtle traps within a Paleogene lacustrine sequence stratigraphic framework, Dongying Depression, Bohai Bay Basin Eastern China. Petrol Sci 17:1–22